Maxwell stress on a small dielectric sphere in a dielectric

Vitaly V. Datsyuk and Oleg R. Pavlyniuk
Department of Physics, Taras Shevchenko National University of Kyiv, Kyiv 01601, Ukraine
(Received 9 October 2014; revised manuscript received 27 January 2015; published 23 February 2015)

Electrically induced normal pressure and tangential stress at the surface of a small dielectric sphere (or cavity) in a dielectric are calculated using the Minkowski, Einstein-Laub, Abraham, and Lorentz forms of the Maxwell stress tensor. Only the Lorentz tensor is in agreement with the following observations: (1) A spherical cavity in a dielectric transforms into a sharp-edge plate perpendicular to the electric field; (2) a liquid drop placed in a medium with a slightly lower refractive index is stretched along the electric field; and (3) there is a torque on a small birefringent sphere. These phenomena cannot be explained by the conventional theory using the Minkowski stress tensor. For example, the Minkowski stress tensor predicts lateral compression of a spherical cavity in a dielectric.

DOI: 10.1103/PhysRevA.91.023826 PACS number(s): 42.50.Wk

I. INTRODUCTION

Mechanical forces of light are important instruments of modern science and technology. These forces are being used in laser tweezers, optical spanners and stretchers, laser traps, optomechanical devices, and systems of laser isotope separation. In laser fusion projects, a target has to be compressed by laser beams. The pressure of sunlight should be taken into account in global positioning systems. Even spacecrafts under light-pressure sails have been proposed.

Calculation of the force acting on a dielectric body in an electromagnetic field is among the fundamental physical problems. This problem was addressed for the first time by James Clerk Maxwell in his famous "Treatise on Electricity and Magnetism" [1]. According to Maxwell, the time-averaged force acting on a body is expressed through the integral over a closed surface surrounding the body:

$$\mathbf{F} = \oint \langle \mathbf{T} \rangle \cdot \hat{\mathbf{n}}\, dA, \tag{1}$$

where $\mathbf{n}$ denotes the external unit vector normal to the surface, $\mathbf{T}$ is the *Maxwell stress tensor*, and brackets denote averaging over time. In the early twentieth century, Maxwell's theory was extended in order to describe the mechanical action of the electromagnetic field in dielectric and magnetic media. The following form of the Maxwell stress tensor was proposed by Lorentz [2]:

$$T_{ij} = \epsilon_0\, E_i\, E_j + \mu_0\, H_i\, H_j - \tfrac{1}{2}(\epsilon_0\, E^2 + \mu_0\, H^2)\, \delta_{ij}. \tag{2}$$

The following form was proposed by Einstein and Laub [3]:

$$T_{ij} = E_i\, D_j + H_i\, B_j - \tfrac{1}{2}(\epsilon_0 E^2 + \mu_0\, H^2)\, \delta_{ij}. \tag{3}$$

The following form was proposed by Minkovski [4]:

$$T_{ij} = E_i\, D_j + H_i\, B_j - \tfrac{1}{2}(\mathbf{E}\,\mathbf{D} + \mathbf{H}\,\mathbf{B})\, \delta_{ij}. \tag{4}$$

The following form was proposed by Abraham [5]:

$$T_{ij} = \tfrac{1}{2}(E_i\, D_j + E_j\, D_i + H_i\, B_j + H_j\, B_i) - \tfrac{1}{2}(\mathbf{E}\,\mathbf{D} + \mathbf{H}\,\mathbf{B})\, \delta_{ij}. \tag{5}$$

Here ϵ_0 and μ_0 are the electric and magnetic constants, respectively, and δ_{ij} is the Kronecker delta. In the microscopic electromagnetic theory by Lorentz [2], the stress tensor of Eq. (2) is a function only of the electric, $\mathbf{E}$, and magnetic, $\mathbf{H}$, fields. Macroscopic approaches gave tensors of Eqs. (3)–(5) in which $\mathbf{D} = \epsilon\, \epsilon_0\, \mathbf{E}$ is the electric displacement, $\mathbf{B} = \mu\, \mu_0\, \mathbf{H}$ is the magnetic induction, and ϵ and μ are the permittivity and permeability of the medium, respectively. Most authors replace $\mathbf{H}$ in Eq. (2) by $\mu_0^{-1}\, \mathbf{B}$ and obtain the tensor called the Amperian [6,7] or Maxwell [8–11] or Raabe-Welsch [12] tensor. This tensor is the same as the Lorentz one if the medium is nonmagnetic ($\mu = 1$, as in the rest of this paper). Also there is no difference between the Minkowski and Abraham stress tensors if the medium is isotropic.

Many efforts have been made to establish the correct form of the stress tensor [6,7,13–17]. At present, Eq. (4) is the generally accepted definition of the Maxwell stress tensor [8,18–31], which is sometimes called the Minkowski stress tensor [7,9,10,12,15,16,32]. However, some researches considered the arguments in its favor as unconvincing [33]. Situations in which different theoretical models give different radiation forces are still being invented to test the theory with experiments. For example, Stallinga used the Minkowski and Amperian stress tensors and calculated different radiation forces on a dielectric slab immersed in a dielectric [10]. Mansaripur and coworkers compared volume electromagnetic-force distributions given by the Lorentz and Einstein-Laub formulations in the cases of propagation of a Gaussian beam through a transparent isotropic dielectric, dielectric slab, and a water droplet [17]. In particular, it was found that the two formulations predict different deformations of a liquid drop.

The aim of this paper is to compare predictions of different forms of the stress tensor with experiments. We examine action of a homogeneous electric field on a dielectric sphere. A similar effect has the radiation pressure on a small sphere when the electrostatic approximation is valid.

II. NORMAL PRESSURE AND TANGENTIAL STRESS

We consider the situation when the electric field is homogeneous inside the sphere, so the divergence of the stress tensor vanishes. In this case, the integral in Eq. (1) over any closed surface inside the sphere is zero. The value of $\mathbf{F}$ is hence determined by surface forces which are measured in Pascals and are expressed through the difference of the Maxwell stress

tensors in two media:

$$\mathcal{F}_j(\mathbf{r}_S) = \left\langle T^{(2)}_{jn}(\mathbf{r}_S)\right\rangle - \left\langle T^{(1)}_{jn}(\mathbf{r}_S)\right\rangle, \tag{6}$$

where $\mathbf{r}_S$ is the radius vector of a point at the surface of the body. The normal component of $\boldsymbol{\mathcal{F}}$ is called the *normal pressure*, $\mathcal{P} = \boldsymbol{\mathcal{F}}\,\hat{\mathbf{n}}$. The tangential component is the *tangential stress* $\mathbf{S}$:

$$\boldsymbol{\mathcal{F}} = \mathcal{P}\,\hat{\mathbf{n}} + \mathbf{S}. \tag{7}$$

The quantity $\mathbf{S}$ is not widely known since it is zero if there are no surface charges σ and the Minkowski, Abraham, or Einstein-Laub tensors are applied.

The components $\mathcal{P}$ and $\mathbf{S}$ of the surface force are readily found using the boundary conditions for the tangential components of $\mathbf{E}$ and $\mathbf{H}$ and normal components of $\mathbf{D}$ and $\mathbf{B}$. If a sphere with the center at the origin of the system of spherical coordinates r, ϑ, ϕ is placed in a constant electric field with $\mathbf{E} = E_0\,\hat{\mathbf{z}}$, then at $\sigma = 0$ we get from Eqs. (4) and (5) that

$$\mathcal{P}_r = \epsilon_1\, C\,(\sin^2\vartheta + \varepsilon\,\cos^2\vartheta), \tag{8a}$$

$$\mathbf{S} = 0, \tag{8b}$$

where $\varepsilon = \epsilon_2/\epsilon_1$, ϵ_2 is the permittivity of the sphere, ϵ_1 is the permittivity of the surrounding medium, and $C = \frac{9\,(\varepsilon-1)}{(\varepsilon+2)^2}\,\frac{\epsilon_0}{2}\,E_0^2$. At the same time, the Lorentz tensor gives

$$\mathcal{P}_r = (\varepsilon + 1)\,C\,\cos^2\vartheta, \tag{9a}$$

$$S_\vartheta = -\,C\,\sin 2\vartheta, \quad S_\phi = 0. \tag{9b}$$

For a time-harmonic field $\mathbf{E} = E_0\,\cos(\omega t)\,\hat{\mathbf{z}}$ the pressure and stress at the surface of a small dielectric sphere are determined by more complicated formulas. However, if ϵ_1 and ϵ_2 are real, then Eqs. (8) and (9) are still valid but with the parameter C divided by 2 (because of time averaging).

III. SPHERICAL CAVITY IN A DIELECTRIC

The surface forces calculated with the stress tensors of Eqs. (2)–(5) can be very different. For example, Fig. 1 shows the forces at the surface of a small spherical cavity in an isotropic nonmagnetic dielectric medium. The top row of the theoretical part of Fig. 1 presents the forces acting on an air bulb in water when $\epsilon_1 = 80.1, \epsilon_2 = 1$. The bottom row was drawn for the relative permittivity $\varepsilon = 0.44$ which corresponds to the experiment [34] with liquid drops in immiscible liquid. The same value of ε is obtained for an empty cavity in a medium with a refractive index of 1.5, the refractive index of many optical materials. There are striking differences between the theoretical columns of Fig. 1. According to Eqs. (8), the electric field pushes the surface of the spherical cavity in the equatorial part. Consequently, the sphere should transform into a prolate spheroid. At very high pressure, it should look like a cylinder or even split into two smaller cavities. Both the Einstein-Laub and Lorentz tensors predict flattering of the spherical cavity. According to the Einstein-Laub model, the electric field pushes the boundaries in the polar regions not affecting the equatorial ones. Therefore, the sphere has to transform into an oblate spheroid and have rounded edges. At very high pressures it tends to be a torus. According to the Lorenz (or Amperian) model, the push of the polar regions of the sphere is concomitant with the tangential pull at the equator of the cavity. These actions could transform the sphere into a plate with sharp edges.

The trend predicted by the Lorentz tensor is in excellent agreement with the experimental data. First, the electric field exerted on a drop placed in immiscible liquid transformed the sphere into a disk [34]. Second, there are a lot of data showing formation of subwavelength structures at the surfaces of transparent dielectrics, semiconductors, and metals under the influence of femtosecond laser pulses [35–37]. If light is

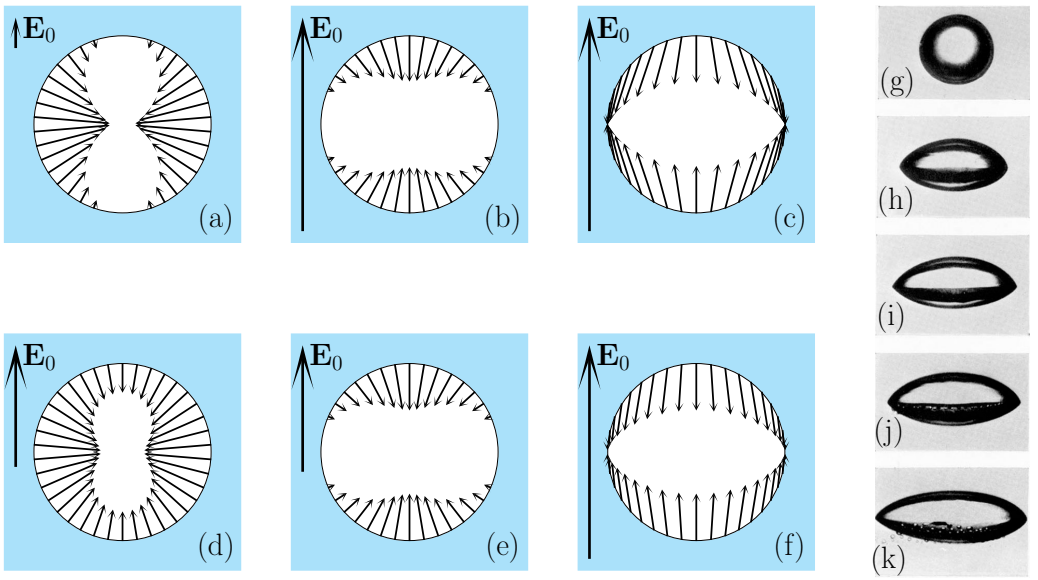

FIG. 1. (Color online) The surface forces calculated with the Minkowski (first column), Einstein-Laub (second column), and Lorentz (third column) stress tensors. The upper row of the theoretical figures (a–c) demonstrates action of a constant electric field on an air bulb in water. The fourth column shows the photographs of a drop of silicon oil in castor oil in constant electric fields [34]. The forces calculated for this experiment are presented in the bottom row of the theoretical figures (d–f). These figures are also for the pressure of light at the surface of an empty spherical cavity in a dielectric with $\epsilon_1 = 2.27$. In all cases, the electric-field vector is directed vertically.

linearly polarized then in most cases grooves are formed in the direction perpendicular to **E**. This phenomenon can be explained by the action of light on nanocavities in a solid [36] if the Lorentz or Einstein-Laub stress tensors are used. The explanation cannot be given when the Minkowski or Abraham stress tensors are applied since they predict formation of channels parallel to **E**.

The above analysis is rather qualitative. The shape of a drop (or bubble) in liquid in a constant electric field is unlikely to be the same as the shape of a void created by femtosecond laser pulses in a solid. To establish these shapes, further efforts are needed. Theoretical estimates of Appendices A and B show that for the parameters specified in the caption to Fig. 1 the deformed sphere is indeed prolate according to the Minkowski stress tensor and oblate according to the Einstein-Laub and Lorentz ones.

IV. DIELECTRIC SPHERE IN A MEDIUM WITH A SIMILAR REFRACTIVE INDEX

Let us consider the forces acting on a dielectric sphere in a medium with a slightly lower refractive index. Figures 2(a)–2(c) show the forces at the surface of a small water droplet in a CO_2 laser field. The forces were calculated neglecting the imaginary part of the refractive index of water $n = 1.173 + i\,0.061$ [38] at an emission wavelength of 10.6 μm and using Eqs. (8) and (9). According to Fig. 2(a), the pressure found with the Minkowski stress tensor is almost independent of the direction of $\mathbf{E_0}$. In contrast, the Einstein-Laub and Lorentz models predict stretching of the droplet along $\mathbf{E_0}$ with slightly different directions of the forces. In experiment [39], Kwok, Wood, and Chang observed distortion, ejection, shattering, and propulsion of water and ethanol 50-μm-radius droplets irradiated by a CO_2 laser pulse. Because of strong absorption of the CO_2-laser emission, water droplets moved in the direction of the laser beam propagation (x direction) and exploded. After explosion, the width of the cloud in the direction of $\mathbf{E}_0$ (z direction) was larger than the diameter $2a$ of the droplet before explosion by a factor of 2.5. Meanwhile, the width of the water cloud in the x direction remained the same as $2a$ and was independent of the z coordinate. These features are in agreement with Fig. 2(c), i.e., the Lorentz stress model.

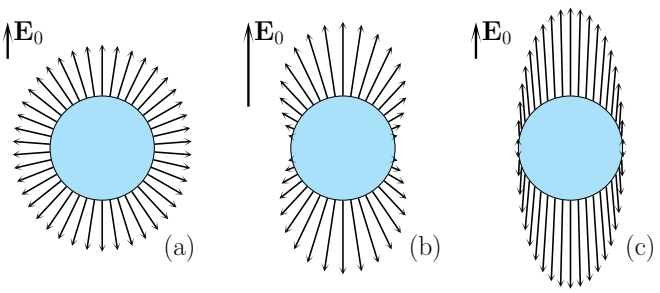

FIG. 2. (Color online) Pressure of CO_2 laser emission on a water droplet calculated with the Minkowski (a), Einstein-Laub (b), and Lorentz (c) stress tensors.

V. BIREFRINGENT SPHERE IN A HOMOGENEOUS ELECTRIC FIELD

The concept of the surface stress can be used to calculate the torque **N** on a small birefringent sphere by using the following definition:

$$\mathbf{N} = \oint_{r=a} [\mathbf{r} \times \mathbf{S}]\, dA. \tag{10}$$

For simplicity, let us consider a sphere with the relative permittivity

$$\varepsilon = \begin{pmatrix} \varepsilon_o & 0 & 0 \\ 0 & \varepsilon_o & 0 \\ 0 & 0 & \varepsilon_e \end{pmatrix} \tag{11}$$

and take

$$\mathbf{E}_0 = E_0 \sin\Theta\, \hat{\mathbf{x}} + E_0 \cos\Theta\, \hat{\mathbf{z}}. \tag{12}$$

The results of the calculations are presented in Table I. This table compares the surface contribution to **N** found from Eq. (10) with the volume contribution:

$$\mathbf{N} = \oint_{r=a} [\mathbf{r} \times \langle \mathbf{T} \rangle] \cdot \hat{\mathbf{n}}\, dA, \tag{13}$$

where $\langle \mathbf{T} \rangle$ is calculated at the internal surface of the sphere. The parameter $\mathbf{N}_0$ in Table I denotes

$$\mathbf{N}_0 = 6\pi a^3\, \epsilon_0\, E_0^2\, \sin(2\Theta) \frac{\varepsilon_e - \varepsilon_o}{(2+\varepsilon_e)(2+\varepsilon_o)}\, \hat{\mathbf{y}}. \tag{14}$$

This value should be divided by 2 for a small sphere in a time-harmonic electric field with the amplitude (12), in accordance with the comment to Eqs. (9). The Lorentz tensor gives the value of **N** recommended by the textbook by Landau, Lifshitz, and Pitaevskii [19]. In Ref. [19], the torque was calculated without using any stress tensor as a cross product of the electric dipole moment of the polarized sphere and the electric-field vector **E** defined at $r \gg a$. The bottom row of Table I presents the value that was found with the Minkowski stress tensor, defined outside the sphere, and the small-particle limit of an extended Lorentz-Mie theory of light scattering [25]. Though the force on any element of the sphere's volume is zero, the Minkowski and Einstein-Laub stress tensors give the senseless volume contributions to **N**. According to Schwinger *et al*, these tensors should be rejected since they do not satisfy condition $T_{ij} = T_{ji}$, "required for the existence of a local conservation law of angular momentum" [20].

Besides the different dependences of N on ϵ_1, the Lorentz and Abraham stress tensors give different distributions of the surface force $\boldsymbol{\mathcal{F}}$. Thus, Fig. 3 presents $\boldsymbol{\mathcal{F}}$ calculated for a small

TABLE I. Torque on a small birefringent sphere.

	Contribution	
Tensor	Surface	Volume
Lorentz	$\mathbf{N}_0$	0
Minkowski	0	$\epsilon_1\, \mathbf{N}_0$
Einstein-Laub	0	$\epsilon_1\, \mathbf{N}_0$
Abraham	$\epsilon_1\, \mathbf{N}_0$	0

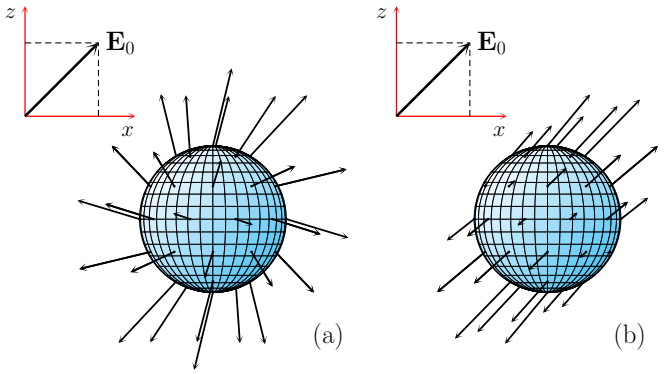

FIG. 3. (Color online) Forces at the surface of a small E44 liquid-crystal sphere in water calculated using the Abraham (a) and Lorentz (b) stress tensors.

E44 liquid crystal (LC) sphere in water. In order to compare the theory with an experiment by Murazawa *et al.* [40] we took $\lambda = 1.064$ nm, for which $n_1 = 1.33$ [38], $n_o = 1.52$, and $n_e = 1.68$ [41]. The angle Θ between the LC optical axes and a linearly polarized electric field $\mathbf{E}$ was set equal to $\pi/4$. Figure 3(b) predicts the possibility of deformation of the sphere that is in a qualitative agreement with the experiment [40] in which a E44 LC drop with a diameter from 1.8 to 3.1 μm was rotated with laser tweezers. Murazawa *et al.* reduced the surface tension of the droplet by adding a small amount of a surfactant to LC. The decrease in the surface tension resulted in a deceleration of the drop rotations that could be explained by "shape modifications of spinning microspheres" [40].

VI. CONCLUSION

In this paper, several forms of the Maxwell stress tensor, known from the early twentieth century, have been used to determine the forces acting on a small dielectric sphere and a spherical cavity in a dielectric. We have considered situations in which different forms of the stress tensors give contradictory results. The agreement between the theory and experiment is excellent for the microscopic (Lorentz) approach and poor for the conventional macroscopic (Minkowski) one. We therefore conclude that the conventional Maxwell-Minkowski theory should not be used to determine deformation or explosion of a dielectric sphere or cavity in an electric field. Thus, we see a failure of the macroscopic electrodynamics. More comparisons of the theory with experiments are badly needed in order to confirm or refute this conclusion.

ACKNOWLEDGMENTS

The authors thank N.G. Zubrilin and Saulius Juodkazis for stimulating discussions.

APPENDIX A: SMALL DEFORMATION OF A SPHERE IN A HOMOGENEOUS ELECTRIC FIELD

Deformation of a liquid sphere can be easily evaluated using the theory of capillary phenomena elaborated by Lord Rayleigh many years ago [42]. This theory explains deviations of the surface of a fluid from a cylindrical or spherical form.

TABLE II. Coefficient q_2 divided by $\frac{2}{3}C$.

Tensor	$\frac{3}{2}q_2/C$
Lorentz	$\varepsilon + 1$
Minkowski, Abraham	$(\varepsilon - 1)\epsilon_1$
Einstein-Laub	$2\epsilon_2 - \varepsilon - 1$

The model of Ref. [42] was very successful even though it considered only small deformations, for example, those of the spherical surface:

$$r = a + \sum_{n=0}^{\infty} \alpha_n P_n(\cos\vartheta), \quad \alpha_n \ll a, \tag{A1}$$

where a is the radius of the unperturbed sphere and P_n are Legendre's polynomials. Here, it is sufficient to assume that deformations are symmetrical about the z axis. Surface curvatures described by Eq. (A1) render the pressure [43]:

$$\mathcal{P}_s = \frac{2\sigma}{a} - \frac{\sigma}{a^2}(2 + \Delta_{\vartheta,\phi}) \sum_{n=0}^{\infty} \alpha_n P_n(\cos\vartheta), \tag{A2}$$

where σ is the superficial tension and $\Delta_{\vartheta,\phi}$ denotes $\frac{1}{\sin\vartheta}\frac{\partial}{\partial\vartheta}(\sin\vartheta\frac{\partial}{\partial\vartheta}) + \frac{1}{\sin^2\vartheta}\frac{\partial^2}{\partial\phi^2}$. The action of the operator $\Delta_{\vartheta,\phi}$ on P_n reduces to the following:

$$\Delta_{\vartheta,\phi} P_n(\cos\vartheta) = -n(n+1) P_n(\cos\vartheta), \tag{A3}$$

so that

$$\mathcal{P}_s = \frac{2\sigma}{a} + \frac{\sigma}{a^2} \sum_{n=0}^{\infty} \alpha_n (n-1)(n+2) P_n(\cos\vartheta). \tag{A4}$$

In equilibrium, there is a balance between the pressures $\mathcal{P}_1$ and $\mathcal{P}_2$ in two media, the surface tension pressure $\mathcal{P}_s$, and the electric-field pressure $\mathcal{P}_r$:

$$\mathcal{P}_2 - \mathcal{P}_1 + \mathcal{P}_r = \mathcal{P}_s. \tag{A5}$$

If deformations are small, the pressure $\mathcal{P}_r$ can be approximated by a value obtained for a sphere of an ideal spherical shape. All the considered stress tensors give $\mathcal{P}_r$ of the same form,

$$\mathcal{P}_r = q_0 + q_2 P_2(\cos\vartheta), \tag{A6}$$

but with different coefficients q_0 and q_2. The latter is presented in Table II. Then, each coefficient α_n can be found from Eq. (A5) owing to the orthogonality of the spherical functions. The coefficient α_0 should be determined together with the pressure $\mathcal{P}_2$ inside the sphere which depends on the volume of the particle:

$$V \simeq \frac{4}{3}\pi(a + \alpha_0)^3 + 4\pi a \sum_{n=1}^{\infty} \frac{\alpha_n^2}{2n+1}. \tag{A7}$$

However, if the medium is inextensible and α_n are small, we can take $\alpha_0 \simeq 0$. There is only one nonzero coefficient in Eq. (A1):

$$\alpha_2 = \frac{q_2 a^2}{4\sigma}, \tag{A8}$$

which determines deformation of the surface. From Eqs. (A8) and (A1), and Table II we find in the particular case of $\varepsilon < 1$ the sphere to be prolate (at $\epsilon_1 > 0$) according to the Minkowski and Abraham stress tensors or oblate according to the Lorentz stress tensor. The sphere should be prolate at $\varepsilon > 2\epsilon_2 - 1$ or oblate at $\varepsilon < 2\epsilon_2 - 1$ according to the Einstein-Laub stress tensor.

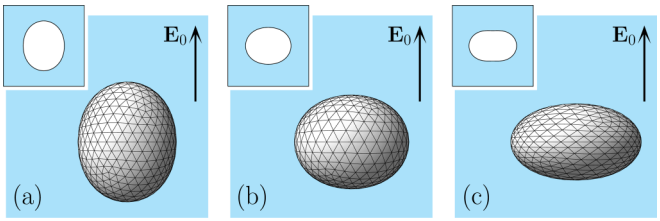

FIG. 4. (Color online) Deformation of a spherical cavity in an elastic dielectric in a homogeneous electric field calculated with the Minkowski (a), Einstein-Laub (b), and Lorentz (c) stress tensors. The insets show the surfaces defined by Eq. (A1) with one nonzero coefficient α_2 equal to 0.1 (a), −0.1 (b), and −0.2 (c).

APPENDIX B: POSITION-BASED SIMULATION OF SHAPE DEFORMATION OF ELASTIC DIELECTRIC BODIES

In order to establish shape deformation of a dielectric body by the surface forces we applied a position-based computation method [44,45]. The position-based approach was combined with the shape matching [45] algorithm. Some details of the calculations are given below. In the simulation, a nonrigid object should be represented by a set of vertices and a set of constraints. We used 642 vertices to model the surface of a sphere. Each vertex has three attributes, namely, the mass, position, and velocity. The two latter attributes are changing due to an external force. In our case, there are 1920 stretch constraints on the distances between vertices within a mesh triangle and one volume constraint. Each constraint is defined through a scalar constraint function which depends on the positions of the definite number (2 or 642) of the vertices (called the cardinality of the constraint) and a stiffness parameter.

Within the position-based approach, calculations are typically executed in two steps. First, a simple explicit forward Euler integration step defines velocities and positions of the vertices. These positions are used only as predictions. Based on these predictions nonpermanent external constraints are generated. Then, the predicted vertex positions are corrected to satisfy constraints. Finally, the corrected positions are used to update the positions and velocities. A static form of the nonrigid object deformed by a steady force is settled down after a number of integration steps.

This method was extended with the shape matching procedure. This approach allows one to simulate dynamics of elastic deformations. In the simulation, the initial configuration of the deformable object should be stored. In each Euler integration step, the predicted positions and velocities of the particles are computed allowing for external forces. Before using internal constraints, goal positions are determined by matching the initial shape with the deformed configuration. The shape matching consists in the search of the best rigid transformation (translation and rotation) that matches initial and predicted positions. Then, each predicted vertex position is pulled toward its goal position using the stiffness parameter. Since the shape matching was used, the stretch constraints were neglected. When calculating the surface forces, we assumed that the electric field is uniform inside the cavity. This approach is rigorous if the cavity has a form of ellipsoid [19].

Results of numeric calculations are presented in Fig. 4, which shows the surface of a deformed cavity in a dielectric as a set of mesh triangles. In each figure, the body axis of rotational symmetry and the electric field are directed vertically. The computed shapes in Figs. 4(a) and 4(b) turned out to be the same as predicted by Eq. (A1) with $\alpha_2 = 0.1$ and −0.1, respectively. In Fig. 4(c) the equatorial part of the cavity is more elongated than that expected from Eq. (A1). When the electric field is increased, cups are formed at the poles of the cavity according to the Einstein-Laub stress tensor.

[1] J. C. Maxwell, *A Treatise on Electricity and Magnetism*, Vol. 2 (Clarendon Press, Oxford, 1873).

[2] H. A. Lorentz, *The Theory of Electrons and its Applications to the Phenomena of Light and Radiant Heat. A Course of Lectures Delivered in Columbia University, New York, in March and April 1906* (Columbia University Press, New York, 1909).

[3] A. Einstein and J. Laub, Über die im elektromagnetischen felde auf ruhende körper ausgeübten ponderomotorischen kräfte, Ann. Phys. **331**, 541 (1908).

[4] H. Minkowski, Die grundgleichungen für die elektromagnetischen vorgänge in bewegten körpern, Nachr. Ges. Wiss. Göttingen (1908), pp. 53–111.

[5] M. Abraham, Zur frage der symmetrie des elektromagnetischen spannungstensors, Ann. Phys. **349**, 537 (1914).

[6] R. N. C. Pfeifer, T. A. Nieminen, N. R. Heckenberg, and H. Rubinsztein-Dunlop, Colloquium: Momentum of an electromagnetic wave in dielectric media, Rev. Mod. Phys. **79**, 1197 (2007).

[7] B. A. Kemp, Resolution of the Abraham–Minkowski debate: Implications for the electromagnetic wave theory of light in matter, J. Appl. Phys. **109**, 111101 (2011).

[8] A. Casner, *Déformations, Manipulations et Instabilités d'Interfaces Liquides Induites par la Pression de Radiation d'une Onde Laser. Thése pour Obtenir le Grade de Docteur* (L'Université Bordeaux 1, Bordeaux, 2002).

[9] S. Stallinga, Energy and momentum of light in dielectric media, Phys. Rev. E **73**, 026606 (2006).

[10] S. Stallinga, Radiation force on a Fabry–Pérot slab immersed in a dielectric, Opt. Express **14**, 1286 (2006).

[11] C. Baxter and R. Loudon, Radiation pressure and the photon momentum in dielectrics, J. Mod. Opt. **57**, 830 (2010).

[12] I. Brevik and S. A. Ellingsen, Comment on "Casimir force acting on magnetodielectric bodies embedded in media", Phys. Rev. A **79**, 027801 (2009).
[13] D. V. Skobeltsyn, The momentum-energy tensor of the electromagnetic field, Phys.-Uspekhi **16**, 381 (1973).
[14] I. Brevik, Experiments in phenomenological electrodynamics and the electromagnetic energy-momentum tensor, Phys. Rep. **52**, 133 (1979).
[15] R. Loudon, S. M. Barnett, and C. Baxter, Radiation pressure and momentum transfer in dielectrics: The photon drag effect, Phys. Rev. A **71**, 063802 (2005).
[16] P. W. Milonni and R. W. Boyd, Momentum of light in a dielectric medium, Adv. Opt. Photon. **2**, 519 (2010).
[17] M. Mansuripur, A. R. Zakharian, and E. M. Wright, Electromagnetic-force distribution inside matter, Phys. Rev. A **88**, 023826 (2013).
[18] V. V. Batygin and I. N. Toptygin, *Problems in Electrodynamics* (Academic Press, New York, 1964).
[19] L. D. Landau, E. M. Lifshitz, and L. P. Pitaevskii, *Electrodynamics of Continuous Media*, Course of Theoretical Physics Vol. 8 (Butterworth, Washington, DC, 1984).
[20] J. Schwinger, J. Lester L. DeRaad, K. A. Milton, and W. Yang Tsai, *Classical Electrodynamics* (Perseus, Reading, 1998).
[21] L. Novotny and B. Hecht, *Principles of Nano-Optics* (Cambridge University Press, Cambridge, 2006).
[22] R. Loudon and C. Baxter, Contributions of John Henry Poynting to the understanding of radiation pressure, Proc. R. Soc. A **468**, 1825 (2012).
[23] R. V. Jones and J. C. S. Richards, The pressure of radiation in a refracting medium, Proc. R. Soc. A **221**, 480 (1954).
[24] J. P. Barton, D. R. Alexander, and S. A. Schaub, Theoretical determination of net radiation force and torque for a spherical particle illuminated by a focused laser beam, J. Appl. Phys. **66**, 4594 (1989).
[25] N. Ji, M. Liu, J. Zhou, Z. Lin, and S. T. Chui, Radiation torque on a spherical birefringent particle in the long wave length limit: Analytical calculation, Opt. Exp. **13**, 5192 (2005).
[26] B. A. Kemp, T. M. Grzegorczyk, and J. A. Kong, Ab initio study of the radiation pressure on dielectric and magnetic media, Opt. Exp. **13**, 9280 (2005).
[27] B. A. Kemp, T. M. Grzegorczyk, and J. A. Kong, Optical momentum transfer to absorbing Mie particles, Phys. Rev. Lett. **97**, 133902 (2006).
[28] E. Yariv, "Force-free" electrophoresis? Phys. Fluids **18**, 031702 (2006).
[29] F. Xu, J. A. Lock, G. Gouesbet, and C. Tropea, Optical stress on the surface of a particle: Homogeneous sphere, Phys. Rev. A **79**, 053808 (2009).
[30] A. Salandrino, S. Fardad, and D. N. Christodoulides, Generalized Mie theory of optical forces, J. Opt. Soc. Am. B **29**, 855 (2012).
[31] Q. Wang, Z. Suo, and X. Zhao, Bursting drops in solid dielectrics caused by high voltages, Nat. Commun. **3**, 1157 (2012).
[32] F. K. Reinhart and G. Boero, Photon energy dependence of the light pressure exerted onto a thin silicon slab, Phys. Rev. B **83**, 165321 (2011).
[33] C. Raabe and D.-G. Welsch, Reply to "Comment on 'Casimir force acting on magnetodielectric bodies embedded in media"', Phys. Rev. A **80**, 067801 (2009).
[34] S. Torza, R. Cox, and S. Mason, Electrohydrodynamic deformation and burst of liquid drops, Phil. Trans. R. Soc. A **269**, 295 (1971).
[35] K. Okamuro, M. Hashida, Y. Miyasaka, Y. Ikuta, S. Tokita, and S. Sakabe, Laser fluence dependence of periodic grating structures formed on metal surfaces under femtosecond laser pulse irradiation, Phys. Rev. B **82**, 165417 (2010).
[36] R. Buividas, L. Rosa, R. Šliupas, T. Kudrius, G. Šlekys, V. Datsyuk, and S. Juodkazis, Mechanism of fine ripple formation on surfaces of (semi) transparent materials via a half-wavelength cavity feedback, Nanotechnology **22**, 055304 (2011).
[37] J. Bonse, J. Krüger, S. Höhm, and A. Rosenfeld, Femtosecond laser-induced periodic surface structures, J. Las. Appl. **24**, 042006 (2012).
[38] M. J. Weber, *Handbook of Optical Materials* (CRC, Boca Raton, 2003).
[39] A. S. Kwok, C. F. Wood, and R. K. Chang, Fluorescence imaging of CO_2 laser-heated droplets, Opt. Lett. **15**, 664 (1990).
[40] N. Murazawa, S. Juodkazis, V. Jarutis, Y. Tanamura, and H. Misawa, Viscosity measurement using a rotating laser-trapped microsphere of liquid crystal, Europhys. Lett. **73**, 800 (2006).
[41] J. Li, C.-H. Wen, S. Gauza, R. Lu, and S.-T. Wu, Refractive indices of liquid crystals for display applications, IEEE/OSA J. Disp. Tech. **1**, 51 (2005).
[42] Lord Rayleigh, On the capillary phenomena of jets, Proc. R. Soc. London **29**, 71 (1879).
[43] L. D. Landau and E. M. Lifshitz, Fluid Mechanics, Course of Theoretical Physics Vol. 6 (Reed Educational and Professional Publishing, Oxford, 1987).
[44] M. Müller, B. Heidelberger, M. Hennix, and J. Ratcliff, Position based dynamics, J. Vis. Commun. Image Repr. **18**, 109 (2007).
[45] J. Bender, M. Müller, M. A. Otaduy, M. Teschner, and M. Macklin, A survey on position-based simulation methods in computer graphics, Comp. Graph. Forum **33**, 228 (2014).